TRPC6 channel translocation into phagosomal membrane augments phagosomal function

Vladimir Riazanski[a,1], Aida G. Gabdoulkhakova[a,1], Lin S. Boynton[a], Raphael R. Eguchi[a], Ludmila V. Deriy[a], D. Kyle Hogarth[a], Nadège Loaëc[b], Nassima Oumata[b], Hervé Galons[c], Mary E. Brown[a], Pavel Shevchenko[a], Alexander J. Gallan[a], Sang Gune Yoo[a], Anjaparavanda P. Naren[d], Mitchel L. Villereal[a], Daniel W. Beacham[e], Vytautas P. Bindokas[a], Lutz Birnbaumer[f,2], Laurent Meijer[b], and Deborah J. Nelson[a,2]

[a]Department of Pharmacological and Physiological Sciences and Department of Medicine, University of Chicago, Chicago, IL 60637; [b]Department of Research and Development, ManRos Therapeutics, Hôtel de Recherche, Centre de Perharidy, 29680 Roscoff, France; [c]Unité de Technologies Chimiques et Biologiques pour la Santé, Université Paris Descartes UMR-S 1022 INSERM 75270, Paris Cedex 06, France; [d]Department of Pediatrics, Division of Pulmonary Medicine and Gastroenterology, Cincinnati Children's Hospital Medical Center, Cincinnati, OH 45229; [e]Molecular Probes, Thermo Scientific, Eugene, OR 97402; and [f]Laboratory of Neurobiology, National Institute of Environmental Health Sciences, Research Triangle Park, NC 27709

Contributed by Lutz Birnbaumer, October 5, 2015 (sent for review April 1, 2015; reviewed by Marie E. Egan and Erich Gulbins)

Defects in the innate immune system in the lung with attendant bacterial infections contribute to lung tissue damage, respiratory insufficiency, and ultimately death in the pathogenesis of cystic fibrosis (CF). Professional phagocytes, including alveolar macrophages (AMs), have specialized pathways that ensure efficient killing of pathogens in phagosomes. Phagosomal acidification facilitates the optimal functioning of degradative enzymes, ultimately contributing to bacterial killing. Generation of low organellar pH is primarily driven by the V-ATPases, proton pumps that use cytoplasmic ATP to load H^+ into the organelle. Critical to phagosomal acidification are various channels derived from the plasma membrane, including the anion channel cystic fibrosis transmembrane conductance regulator, which shunt the transmembrane potential generated by movement of protons. Here we show that the transient receptor potential canonical-6 (TRPC6) calcium-permeable channel in the AM also functions to shunt the transmembrane potential generated by proton pumping and is capable of restoring microbicidal function to compromised AMs in CF and enhancement of function in non-CF cells. TRPC6 channel activity is enhanced via translocation to the cell surface (and then ultimately to the phagosome during phagocytosis) in response to G-protein signaling activated by the small molecule (R)-roscovitine and its derivatives. These data show that enhancing vesicular insertion of the TRPC6 channel to the plasma membrane may represent a general mechanism for restoring phagosome activity in conditions, where it is lost or impaired.

phagosome | TRPC6 | alveolar macrophage | cystic fibrosis | roscovitine

Chronic infection and inflammation in the airways in cystic fibrosis (CF), as well as chronic obstructive pulmonary disease (COPD), tuberculosis, and asthma are now among the most common chronic diseases. Pulmonary infection associated with these diseases has historically been treated with antibiotics that kill bacteria but also select for development of resistance in the pathogen in the chronically infected lung (1, 2). One solution to antimicrobial drug resistance is to target the host rather than the pathogen. This strategy necessitates finding alternative targets or signaling strategies amplifying or restoring bactericidal capacity in the cells charged with the task of resolving chronic infection.

Mononuclear phagocytes orchestrate the innate immune response in the lung through the combinatorial interplay between the phagocytic uptake and killing of bacterial invaders, clearance of apoptotic cells, antigen presentation, and secretion of vesicle-bound signaling molecules to recruit help in the resolution of infection. Ionic fluxes across the phagosomal membrane that encloses the pathogen produce a hostile acidic environment developed through the action of a V-ATPase proton translocation. However, a positive intraphagosomal membrane potential generated by proton translocation minimizes the proton content of the phagosome. An influx of Cl^- via Cl^- channels reduces the membrane potential generated by the proton pump, thereby, allowing maximal acidification of the phagolysosomal compartment, which in turn maximizes the activation of lysosomal degradative enzymes, generation of hypochlorous acid, and consequent bacterial killing (3, 4). We have previously demonstrated that murine alveolar macrophages (AMs) use the anion channel cystic fibrosis transmembrane conductance regulator (CFTR) as a Cl^- permeation pathway in the phagosomal membrane. In CF, loss of functional CFTR in the AM alkalinizes the phagosomal lumen and allows antimicrobial-resistant bacterial pathogens to survive macrophage surveillance.

Not all tissue macrophages use CFTR as a charge compensation pathway in phagolysosomal acidification (4). In fact, recent data suggest that multiple V-ATPase charge-shunt pathways can exist in diverse macrophage lineages (5) via lysosomal recruitment and

Significance

Historically, pulmonary infections treated with antibiotics killed bacteria while selecting for the unintended development of pathogenic resistance. One strategy to circumvent antibiotic resistance in pulmonary infection involves targeting the host phagosome and augmenting its function. To such an end, we have identified several small molecules, (R)-roscovitine and its derivatives, which restore microbicidal activity to compromised alveolar macrophages in cystic fibrosis (CF) and enhance function in non-CF cells. The compounds utilize G protein signaling pathways that mobilize TRPC-6 channels to the plasmalemma and subsequent phagosomal membrane formation that engulfs the bacterium. The plethora of GPCRs in resident pulmonary macrophages linked to ion channel function provides a rich source for potential therapeutic approaches to macrophage-mediated disease.

Author contributions: V.R., A.G.G., V.P.B., and D.J.N. designed research; V.R., A.G.G., R.R.E., L.V.D., D.K.H., N.L., P.S., A.J.G., S.G.Y., and A.P.N. performed research; N.O., H.G., M.L.V., D.W.B., V.P.B., L.B., and L.M. contributed new reagents/analytic tools; V.R., A.G.G., L.S.B., R.R.E., L.V.D., N.L., M.E.B., and V.P.B. analyzed data; V.R., A.G.G., and D.J.N. wrote the paper; and L.B. generated and provided the TPRC6-deficient mice and experimental strategies for the $Ca2^+$ experiments, and contributed significant suggestions to manuscript, as well as figure design and revisions.

Reviewers: M.E.E., Yale University School of Medicine; and E.G., University of Duisburg-Essen.

Conflict of interest statement: L.M. is an employee and shareholder of ManRos Therapeutics. L.M. is a founder of ManRos Therapeutics and a member of its scientific advisory board. L.M. is a co-inventor on the roscovitine patent. H.G. is a consultant for and shareholder of ManRos Therapeutics. H.G. is a founder of ManRos Therapeutics and a member of its scientific advisory board. N.O. is an employee of ManRos Therapeutics. N.L. is an employee of the CNRS, funded on a grant from ManRos Therapeutics.

Freely available online through the PNAS open access option.

[1]V.R. and A.G.G. contributed equally to this work.

[2]To whom correspondence may be addressed. Email: Birnbau1@gmail.com or nelson@uchicago.edu.

This article contains supporting information online at www.pnas.org/lookup/suppl/doi:10.1073/pnas.1518966112/-/DCSupplemental.

membrane insertion upon particle uptake. This observation led us to search for possible alternative charge-shunt pathways in pulmonary macrophages and how they might be activated or targeted to the maturing phagosome. Could a pharmacological tool circumvent the defect in CF AMs and activate alternative pathways to rescue both organellar acidification and bactericidal activity in cells expressing mutations in CFTR? Such a tool might activate parallel charge-shunt pathways used in peritoneal macrophages for maximum acidification, thereby allowing them to clear bacteria independently of CFTR expression as well as amplify the microbicidal response in the presence of functional CFTR. The transport proteins and channels active in peritoneal macrophage bacterial clearance have not been described but may involve a K^+/H^+ exchanger important in promoting excitatory synaptic vesicle filling (6) or a cation channel moving positive charge out of the phagolysosomal compartment, as has been suggested for macrophage cell lines (7).

We began our investigations pursuing a novel pharmacological strategy to identify compounds that would resolve bacterial infection in the CF lung without the use of antimicrobials. We picked a cellular defect in CF because of the availability of animal models and extended our observations to non-CF human pulmonary cells. We designed screening assays of phagosome function, which could be used in a clinical setting as both diagnostic and investigational tools. We interrogated host function by studying surface receptor-mediated mechanisms that might provide parallel signaling pathways in subcellular organellar function in the resolution of disease.

We report that a series of small molecules first identified in chemotherapeutics, (R)-roscovitine [2-(R)-(1-ethyl-2-hydroxyethylamino)-6-benzylamino-9-isopropylpurine] and its derivatives, restore microbicidal function to compromised AMs in CF and enhance function in non-CF cells. The compounds use a G protein-mediated signaling pathway, which results in the mobilization of transient receptor potential canonical-6 (TRPC6) calcium-permeable, nonselective cation channels to the plasma membrane and subsequently to the phagosomal membrane. Members of the TRP channel family have been implicated in a number of critical phagocytic functions, including particle uptake, migration, and reactive oxygen species (ROS) production (5, 8–11). Numerous studies (12–15) have suggested TRP channels as potential targets for the development of therapies in pulmonary inflammation because of their abundant and diverse cellular expression throughout the respiratory tree. Although TRPC6 channels have been previously identified in lung macrophages and shown to be up-regulated in COPD, their precise role in the pathophysiology of the disease is yet to be determined (16). Perhaps more relevant to our study, a TRPC6-mediated Ca^{2+} influx is increased in human CF airway epithelial cells, possibly because of a functional association between CFTR and TRPC6 that is lost in CF (17), with unknown consequences. To our knowledge, this study is the first to associate TRPC6 channels a specific drug-targeting strategy for the resolution chronic pulmonary infection.

Results

Our goal was to identify compounds that could switch defective CF macrophages to a state of enhanced microbial killing. The phagocytic sequence can be divided into three stages: recognition by and binding of a particle to a surface receptor, internalization and sequestration of the particle by an actin-dependent process, and finally, conversion of the phagosomal compartment into a microbicidal environment. The assay used to screen for innate immunity enhancers targeted the final step in the process. Phagosomal acidification is a prerequisite for efficient bacterial killing (18); thus, our first screen was for compounds that enhanced phagosomal acidification upon internalization of bioparticles conjugated to the pH-sensitive dye pHrodo, as depicted in Fig. 1. Human AMs were isolated from bronchoalveolar lavage (BAL), plated and cultured in multiwell plates, and exposed to dye-conjugated lyophilized *Escherichia coli* particles for phagocytic uptake (Fig. 1*A*). The kinetics of phagosomal uptake and acidification were read in a plate reader over a period of 3 h, during which time cells continued to take up particles as well as acidify. In a screen of kinase modulatory small molecules, (R)-roscovitine and related purines were identified as candidate compounds for significantly enhancing acidification of phagosomal pH over that observed in untreated cells (Fig. 1 *B* and *C*). Negative controls in the screen included the V-ATPase inhibitor bafilomycin (Baf) and the potent phospholipase C inhibitor edelfosine (ET-18-OCH_3), previously shown to prevent phagocytic uptake at the level of actin assembly (19). The *N*-formyl peptide, fMLF, which binds to a GPCR, inducing mobilization of intracellular Ca^{2+}, production of ROS, and chemotaxis in human and murine phagocytes, was used as a positive control. The fMLF

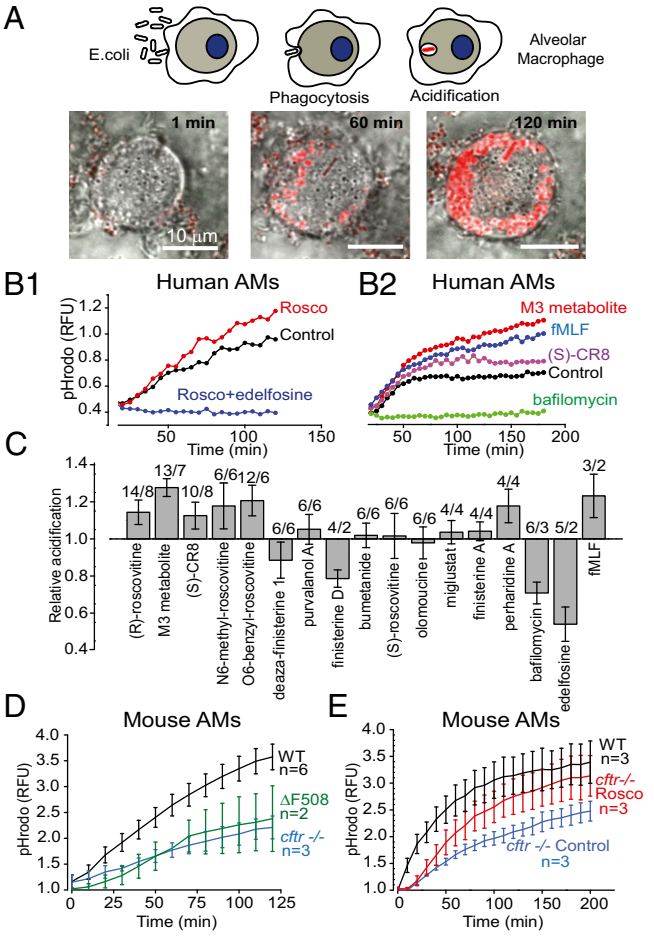

Fig. 1. (R)-roscovitine (rosco) and related derivatives potentiate phagosomal acidification in human AMs. (*A*) Schematic of phagocytosis and pHrodo red-labeled lyophilized *E. coli* particle acidification. Merged differential interference contrast (DIC) and fluorescence images for AMs following a 120- to 200-min loading with the pH sensor pHrodo red-labeled particles. (Scale bars, 10 μm.) (*B1* and *B2*) Kinetics of acidification for representative compounds in human AMs isolated from BAL. Data in *B1* and *B2* are representative drug response comparisons in AMs obtained from two patients. (*C*) Comparative effects of various compounds on relative acidification levels in human AMs measured in a plate reader after 120 min of bioparticle feeding. Data summary from two to eight patients for each compound tested at 10 μM; *n* = experiments/BAL above each bar. Experimental populations for all figures are summarized in Table S4. (*D*) Comparison of the relative acidification time course obtained from $cftr^{+/+}$ (wild-type), $cftr^{-/-}$, and ΔF508 AMs. (*E*) Comparison of acidification time course from $cftr^{+/+}$ (wild-type) AMs and $cftr^{-/-}$ AMs in the presence and absence of 20 μM (R)-roscovitine. Experiments done in triplicate were averaged and presented as means ± SEM; *n* = mice.

receptor family forms a class of proteins that enhance the innate immune response and have been proposed as viable targets for therapeutic drug development (20). (R)-roscovitine (shortened to roscovitine or "rosco" in the figures), first identified as a cyclin-dependent kinase (CDK) inhibitor, is also capable of resolving inflammation (see ref. 21 for review). The structures and kinase inhibitory activity of (R)-roscovitine and related molecules identified in the screen are given in Fig. S1 and Tables S1 and S2. Some molecules triggering enhanced acidification displayed little or no kinase inhibitory activity [e.g., M3 (oxo-roscovitine), the major hepatic (R)-roscovitine biodegradation metabolite, N6-methyl-roscovitine, "O6-benzyl-roscovitine"], whereas some potent kinase inhibitors [deaza-finisterine, finisterine A and D, (S)-roscovitine, olomoucine] were unable to induce acidification, suggesting that kinase inhibition is unlikely to contribute to the organellar acidification properties of (R)-roscovitine and its analogs. The acidification aspect of the screen was replicated using AMs isolated from *cftr*$^{+/+}$ (wild-type), *cftr*$^{-/-}$, and ΔF508 mice (Fig. 1*D*). As in previously published studies (3, 4), cells either lacking CFTR expression or expressing the mutant protein showed decreased acidification compared with *cftr*$^{+/+}$ cells. Treatment of *cftr*$^{-/-}$ cells with (R)-roscovitine (20 μM) restored acidification to a level not significantly different from that observed in *cftr*$^{+/+}$ cells (Fig. 1*E*). Clearly, a parallel non-CFTR–related acidification pathway exists in *cftr*$^{-/-}$ macrophages.

(R)-Roscovitine Rescues Phagosomal Acidification in the Absence of Functional CFTR Expression: Direct Video Observations. An increase in total acidification registered in the plate assay could be because of an increase in particle uptake, an increase in acidification in unitary phagosomes, or both. To resolve the relative contribution of both pathways to the response, we examined the time course and acidification of individual phagosomes in the presence of candidate compounds, as well as average particle uptake per cell in single-cell live video microscopy (Fig. 2*A*) on murine cells, where we could manipulate the functional expression of CFTR and, therefore, phagosomal acidification. These experiments examined whether: (*i*) (R)-roscovitine enhanced phagosomal acidification, particle uptake, or both; and (*ii*) whether (R)-roscovitine could rescue the acidification/microbicidal defect in *cftr*$^{-/-}$ and ΔF508 AMs independent of CFTR expression. Cells were exposed to zymosan particles doubly conjugated to the content marker Rhodamine-green and the pH indicator, pHrodo red, in the presence and absence of (R)-roscovitine (20 μM). We examined and compared the relative time course of acidification for all genotypes (Fig. 2*B*) and compared the rescue of acidification by (R)-roscovitine in AMs from ΔF508 and *cftr*$^{-/-}$ animals (Fig. 2 *C* and *D*). The ratio of pHrodo red to rhodamine green fluorescence was converted to pH using an in situ calibration protocol (Fig. 2*E*) and used to compare phagosomal pH data across genotypes in Fig. 2*F*. (R)-roscovitine enhanced phagosomal acidification by 1.5 pH units in ΔF508 AMs (pH 5.9 to pH 4.4) and a similar amount in the *cftr*$^{-/-}$ cells (pH 6.2 to 4.6). No significant change in phagocytic index was observed for *cftr*$^{+/+}$ or ΔF508 AMs (Table S3) following (R)-roscovitine treatment. The average number of ingested particles per cell was 2.48 ± 0.07 ($n = 551$) before and 2.25 ± 0.07 ($n = 409$) after (R)-roscovitine treatment for *cftr*$^{+/+}$, and 1.93 ± 0.12 ($n = 316$) before and 2.10 ± 0.10 ($n = 387$) after (R)-roscovitine treatment for ΔF508 AMs. Surprisingly, however, in addition to restoring acidification, (R)-roscovitine also increased the cellular activation index (the percentage of phagocytizing cells) in ΔF508 AMs from 44% to 69%, which was equivalent to that seen in *cftr*$^{+/+}$ cells (73%).

(R)-Roscovitine Rescues Bacterial Killing in a CFTR- and Kinase-Independent Manner. Given the tight coupling between phagosomal acidification, host-signaling response, lysosome fusion, and most importantly, bactericidal activity (3, 22, 23), we examined whether (R)-roscovitine could restore bacterial killing profiles in AMs from *cftr*$^{-/-}$ and ΔF508 CFTR-expressing mice. In these experiments, cultured AMs were exposed to (R)-roscovitine (20 μM) for 15–30 min before exposing cells to live, DsRed-expressing *Pseudomonas aeruginosa.* Cells were allowed to ingest bacteria in the continued presence of (R)-roscovitine and were observed by live-cell video microscopy over a 6-h period for an increase in fluorescence indicative of bacterial growth, either in the phagosome or in the cytoplasm following escape from the phagosome (Fig. 3 *A*–*C*). Intracellular bacterial growth as a function of genotype is compared in Fig. 3 *D*–*F*. As expected, both ΔF508 CFTR and *cftr*$^{-/-}$ cells showed a reduction in bacterial killing, in contrast to wild-type, *cftr*$^{+/+}$ cells (Fig. 3*D*). (R)-roscovitine significantly rescued bacterial killing in ΔF508 CFTR-expressing cells (Fig. 3*E*), as well as in *cftr*$^{-/-}$ cells (Fig. 3*F*) to levels similar to that seen in *cftr*$^{+/+}$. The CDK kinase-inactive derivative of (R)-roscovitine, M3, also rescued bacterial killing, validating that (R)-roscovitine rescue of bacterial killing is independent of its activity as a kinase inhibitor. Neither (R)-roscovitine nor its derivative M3 at a concentration of 20 μM

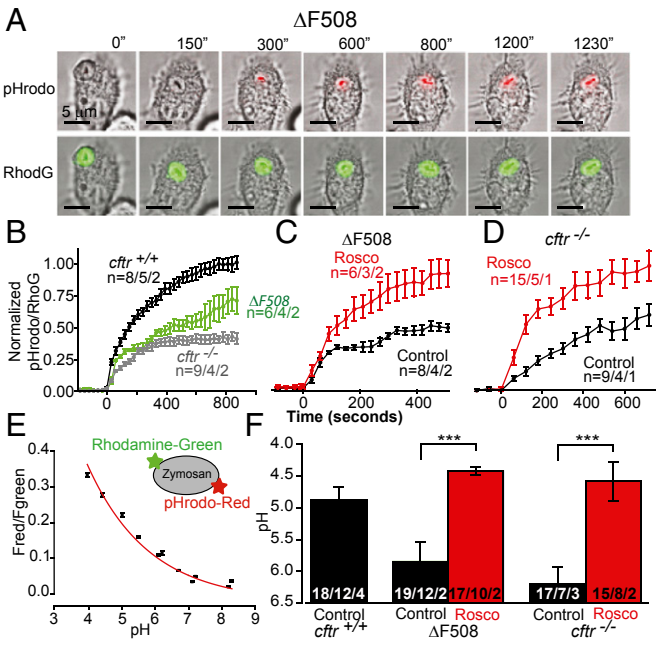

Fig. 2. Rescue of phagosomal acidification in murine ΔF508 and *cftr*$^{-/-}$ AMs by (R)-roscovitine. (*A*) A representative murine (ΔF508) cell loaded with doubly conjugated pHrodo red and rhodamine green zymosan particles and observed over time. (*B*) Representative averaged time course of phagosomal acidification for the three genotypes in the absence of drug. (*C*) Comparative time course of acidification in ΔF508 and (*D*) *cftr*$^{-/-}$ AMs in the presence and absence of 20 μM (R)-roscovitine. Cells were exposed to drug for 20 min before the addition of zymosan. Data are presented as means of fluorescence ± SEM and were normalized to fluorescence ratio changes observed in untreated control cells in *B* and to the (R)-roscovitine–treated cells in *C* and *D*. (*E*) pHrodo red and rhodamine green fluorescence ratios (Fred/Fgreen) were calibrated in vivo using a three-component buffer at the indicated pH values in digitonin-permeabilized cells. (*F*) Summary data using endpoint acidification values obtained in experiments similar and in addition to those in *B*–*D*. The endpoint of each treatment was determined as the average of last three time points on the acidification curves. Values for pH were determined by interpolation. The average pH in phagosomes was: *cftr*$^{+/+}$ 4.87 ± 0.2; ΔF508 5.85 ± 0.31 and 4.42 ± 0.07 following (R)-roscovitine treatment; *cftr*$^{-/-}$ 6.2 ± 0.27 and 4.58 ± 0.31 following (R)-roscovitine treatment. Data in *B*–*F* expressed as mean ± SEM; n = particles per cells per mice. Significance level: ***$P < 0.001$ (two-way ANOVA).

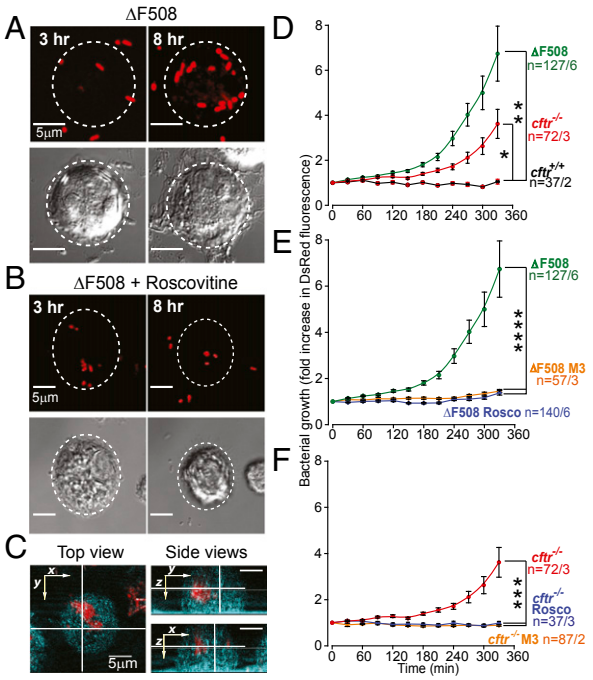

Fig. 3. (R)-Roscovitine rescues bacterial killing defects in $cftr^{-/-}$ and ΔF508 AMs. (*A*) Representative fluorescence and DIC images of an outlined cell from a ΔF508 mouse under control conditions and (*B*) in the presence of (R)-roscovitine with ingested bacteria at 3 and 8 h. Note: bacteria in *B* appear smaller because of lower magnification. (*C*) Intracellular localization of DsRed-expressing bacteria was confirmed by 3D reconstruction of confocal *z*-stacks of bacterial fluorescence and cellular reflection/backscatter. Orthogonal views inside one cell are shown in two right panels, confirming intracellular bacterial growth. (*D*) Summary data from at least three separate experiments comparing bacterial growth over time assayed as mean DsRed fluorescence intensity ($\lambda = 607 \pm 20$ nm) and compared across genotypes, (*E*) in ΔF508 AMs in the presence and absence of (R)-roscovitine or M3 metabolite, 20 μM, and in (*F*) in $cftr^{-/-}$ AMs in the presence and absence of either (R)-roscovitine or M3 metabolite, 20 μM. Bacterial growth in $cftr^{-/-}$ cells compared with growth in ΔF508 AMs was not significantly different across all time points. Data are presented as means of fluorescence intensities ± SEM. Significance levels determined by one-way ANOVA (*$P < 0.05$, **$P < 0.01$, ***$P < 0.001$, and ****$P << 0.0001$) were determined for six last time points in *E* and four last time points in *F*; *n* = cells per mice.

revealed either direct bactericidal or bacteria static activity in cell free assays (Fig. S2).

Patch Clamp Evidence That (R)-Roscovitine Activates a TRPC6 Conductance in AMs Independent of CFTR Expression. Postulating that (R)-roscovitine might open an unidentified ion channel in the plasma membrane that would eventually be incorporated into the phagosomal membrane during the uptake of cargo, we performed whole-cell voltage-clamp experiments on cultured murine AMs isolated from $cftr^{+/+}$, $cftr^{-/-}$, and ΔF508 animals. Experiments were carried out using solutions in which the equilibrium potential for Cl^- was set to −31 mV, allowing us to differentiate anion from cation selective currents. We monitored current activation (Fig. 4*A*) following a 10-μM (R)-roscovitine exposure and observed a lag of ∼3–5 min before a current increase was detected at a depolarized potential of +100 mV. This lag suggested that (R)-roscovitine was not activating channels directly. Drug-induced current activation while maintaining the whole-cell configuration was observed inconsistently, with variable results in both activation time course and current amplitude. We attributed this to the possible loss of a cellular signaling factor integral to the (R)-roscovitine response via the whole-cell patch pipette. To avoid possible current rundown (as seen in Fig. 4*A*), we performed a population study comparing currents immediately after establishing the whole-cell configuration in cells across genotypes in the presence and absence of (R)-roscovitine (Fig. 4 *B–D*). In the presence of (R)-roscovitine, AMs of the three genotypes displayed current activation in the voltage range between −50 and +100 mV, exhibiting a reversal potential of ∼0 mV. Thus, the (R)-roscovitine sensitive current was: (*i*) not a Cl^- selective conductance, (*ii*) was likely a nonselective cation current with significant inward rectification, and furthermore, (*iii*) was not dependent on CFTR expression. (R)-roscovitine–activated currents were similar in selectivity to those reported (24) for the heterologously expressed recombinant human TRPC6 channels: nonselective cation channels that are Ca^{2+}-permeable. Expression of TRPC6 channels has been reported in human AMs and is known to be elevated in AMs originating from patients who are smokers and from those diagnosed with COPD (16). TRPC6 channels are gated through direct interaction with diacylglycerol (DAG) or its membrane permeant analog 1-oleoyl-2-acetyl-*sn*-glycerol (OAG). To explore the possibility that TRPC6 channels could contribute to the (R)-roscovitine currents, OAG-induced currents were recorded from $cftr^{+/+}$ AMs in standard Na^+ and K^+ containing bath and pipette solutions (Fig. 4*E*). The OAG-induced current voltage (I-V) relationship was similar to that seen with (R)-roscovitine

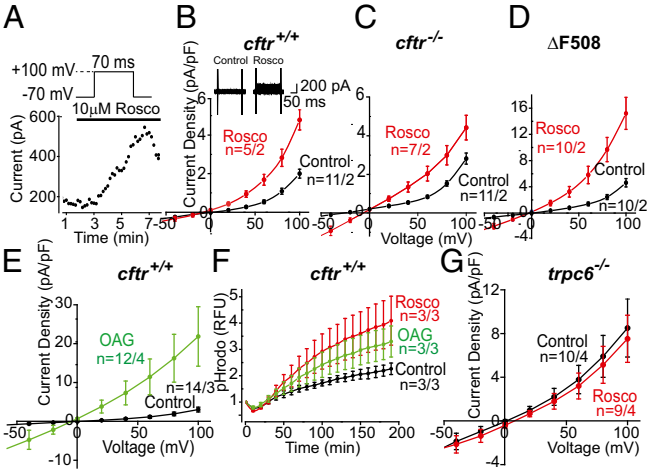

Fig. 4. (R)-Roscovitine activates TRPC6 conductance in murine AMs. (*A*) Time course of whole-cell current activation following treatment with (R)-roscovitine. Cells were depolarized to +100 mV for 70 ms from a holding potential of −70 mV at 10-s intervals. Peak current at +100 mV is plotted as a function of time following (R)-roscovitine addition to the bath. (*B*) Average current-voltage (I-V) relationship from wild-type ($cftr^{+/+}$) cells examined in either control or 20 μM (R)-roscovitine-containing solutions. (*Inset*) Representative whole-cell voltage-clamp recording of AM in the initial absence of drug and subsequent application of (R)-roscovitine. (R)-roscovitine-associated whole-cell currents were elicited during a series of test pulses from −100 to +100 mV in 20-mV increments from holding potential −40 mV. (*C*) Average I-V relationship from $cftr^{-/-}$ cells examined in control solution or solution containing 20 μM (R)-roscovitine, (*D*) from ΔF508 cells examined in control or solution containing 20 μM (R)-roscovitine, and from (*E*) wild-type ($cftr^{+/+}$) cells examined in control solution or in solution containing 100 μM OAG. (*Inset*) Representative whole-cell voltage-clamp recording of wild-type AMs in bath solution with and without OAG. Voltage protocol as in *B*, above. (*F*) Plate-reader comparison of the time course and amplitude of acidification (in arbitrary units) in wild-type AMs as a function of ingested pHrodo red-conjugated *E. coli* under control conditions (black), with 20 μM (R)-roscovitine (red), or 100 μM OAG (green). Experiments were performed in triplicate and averaged for each mouse with three mice per treatment. (*G*) Average I-V relationship recorded from *trpc6* $^{-/-}$ cells examined in control and 20 μM (R)-roscovitine containing bath solution. Solution compositions for bath and pipette in each experimental condition are given in *SI Materials and Methods*; number of mice in each experiment is given in Table S4 and indicated in the plots as *n* = cells per mice.

(Fig. 4 *B–D*). OAG current density was much larger than that observed with (R)-roscovitine because of the fact that OAG activates channels directly, whereas (R)-roscovitine activation is indirect.

Plasma membrane TRPC6 channels incorporated into the nascent phagosomal membrane upon particle uptake would facilitate cation loss from the lumen, both divalent and monovalent, augmenting a Cl^--dependent charge-shunt pathway, if present. The two charge-shunt pathways acting in concert would be expected to enhance phagosome acidification as seen in the non-CF human screening data (Fig. 1). Both (R)-roscovitine and OAG significantly enhanced acidification following bioparticle uptake compared with control (Fig. 4*F*). Thus, either a Cl^- entry pathway (control) or the cation efflux [OAG/(R)-roscovitine] pathway could act alone to shunt V-ATPase–mediated accumulation of positive charge in the lumen.

To verify that (R)-roscovitine–activated currents were dependent upon TRPC6 expression, we carried out voltage-clamp experiments on AMs isolated from *trpc6*$^{-/-}$ animals. As seen in Fig. 4*G*, (R)-roscovitine failed to induce current activation in the absence of TRPC6 expression. The kinase inactive (R)-roscovitine derivative, M3, showed a similar current-activation profile and was dependent upon TRPC6 expression as well (Fig. 5 *A* and *B*). To further establish that (R)-roscovitine activates currents indirectly through a second messenger mechanism active at the internal surface, we performed cell-attached single-channel experiments in which the agonists M3 and OAG were added to the bath solution outside the pipette while currents across the chemically inaccessible patch membrane were observed. Single-channel open-state probability was compared under control conditions and in the presence of either M3 or OAG (Fig. 5*C*) with a significant increase observed in the presence of either agonist (Fig. 5*E*). Single-channel I-V relationships for the channels activated in the presence of the bath applied agonists were similar for M3 and OAG, and the observed values were consistent with the single-channel conductance of 35 pS reported for TRPC6 in the literature (25, 26) (Fig. 5*D*). These data demonstrate that (R)-roscovitine activates channels indirectly and, furthermore, current activation is dependent upon TRPC6 expression.

Translocation of TRPC6 to the Plasma Membrane upon Exposure to (R)-Roscovitine and Subsequent Incorporation into Phagosomal Membranes. We verified that TRPC6 is expressed in murine macrophage-like J774 cells in experiments using an antibody to the C-terminal cytoplasmic domain, α-hTRPC6$_{796–809}$, as shown in Fig. 6*A* and Fig. S4. Significant TRPC6 expression was observed for murine AMs as well (Fig. S3 *B* and *C*). TRPC6 was diffusely distributed throughout the cytoplasm of resting cells in a clustered manner suggesting vesicle localization. Although TRPC6 localization around phagocytosed zymosan particles can be visualized in immunocytochemical images, direct proof that TRPC6 is incorporated into the phagosomal membrane is seen at high resolution in the immuno-electron micrographs in Fig. 6 *B*, *1*. Immunogold labeling of isolated phagosomal membrane fragments from (R)-roscovitine-treated cells using α-hTRPC6$_{796–809}$ demonstrated significant TRPC6 localization over that seen in the control membranes (Fig. 6 *B*, *2*), indicating clustering and possible targeting to membrane lipid rafts as has been reported for a number of TRP channels (27–31). Recent data demonstrate that hypoxia induces TRPC6 translocation to caveolin- and sphingolipid-rich membrane rafts in human pulmonary artery smooth-muscle cells (32).

Direct Measurement of Ca^{2+} Loss from Phagosomes Following Activation of TRPC6. The ionic content of the phagosome initially reflects that of the extracellular solution: high in Ca^{+2}, Na^+, and Cl^-. Activation of TRPC6 channels in the phagosomal membrane would permit the efflux of Ca^{2+} as well as Na^+ from the phagosomal lumen down their electrochemical gradient. To evaluate this hypothesis, we

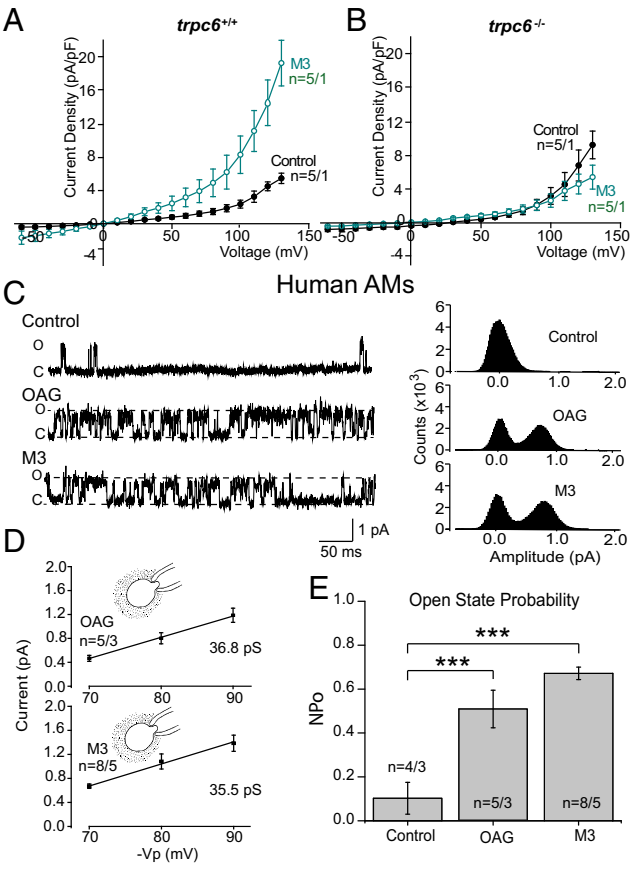

Fig. 5. The (R)-roscovitine derivative, M3, activates TRPC6 channels in human and murine AMs using an internal pathway. (*A*) Peak I-V relationships recorded from wild-type cells examined in control (n = 5 cells) and in 10 μM M3 containing bath solution (n = 5 cells). M3-stimulated whole-cell currents were elicited during a series of test pulses from −60 to +140 mV in 10-mV increments from a holding potential of −40 mV. (*B*) I-V relationships from *trpc6*$^{-/-}$ cells examined in control bath solution (n = 5 cells) and in solution containing 10 μM M3 (n = 5 cells). (*C*) Representative cell-attached single channel recordings in human AMs of OAG and M3 elicited currents with corresponding all-points amplitude histograms. Recordings were taken with 250 nM apamin, 10 μM Pyr10, 10 μM GlyH 101, and 200 μM DIDS in the pipette solution to block contaminating channel currents. (*D*) Single-channel I-V relationships and single-channel conductance in human AMs detected in the presence of either M3 (10 μM) or OAG (50 μM) outside of the pipette. Cell-attached patches were not exposed to the agonist in the bath. Mean single-channel amplitude was determined from three patches at each voltage. Calculated single-channel conductance was 36.8 pS for OAG treatment and 35.5 pS for M3 treatment. (*E*) Summary of single-channel open-state probabilities recorded with bath applied OAG or M3 in human AMs as in *C*. Open-state probabilities were 0.10 ± 0.07 (n = 4 patches) under control conditions, 0.67 ± 0.02 (n = 8 patches) in the presence of M3, and 0.50 ± 0.08 (n = 5 patches) in the presence of OAG. All records were obtained at V_p = +80 mV. Significance level: ***P < 0.001 (two-way ANOVA). Solution composition for bath and pipette in each experimental condition are given in *SI Materials and Methods*; number of mice and patient BAL samples in each experiment is given in Table S4 and indicated in the plots as n = cells per mice or cells per BAL.

exposed murine AMs to zymosan particles, which had been saturated in an extracellular solution containing both the fluorescent Ca^{2+}-sensitive dye, calcein (100 μM), and the protonophore, FCCP (10 μM). Cells were allowed to take up the zymosan particles and calcein fluorescence was measured in the absence of TRPC6 activation. Exposure of the cells to an extracellular solution containing 100 μM La^{3+} to block the plasma membrane Ca^{2+}-permeable channels and 100 μM OAG to activate the phagosomal TRPC6 channels, resulted in the loss of Ca^{2+}-dependent calcein fluorescence

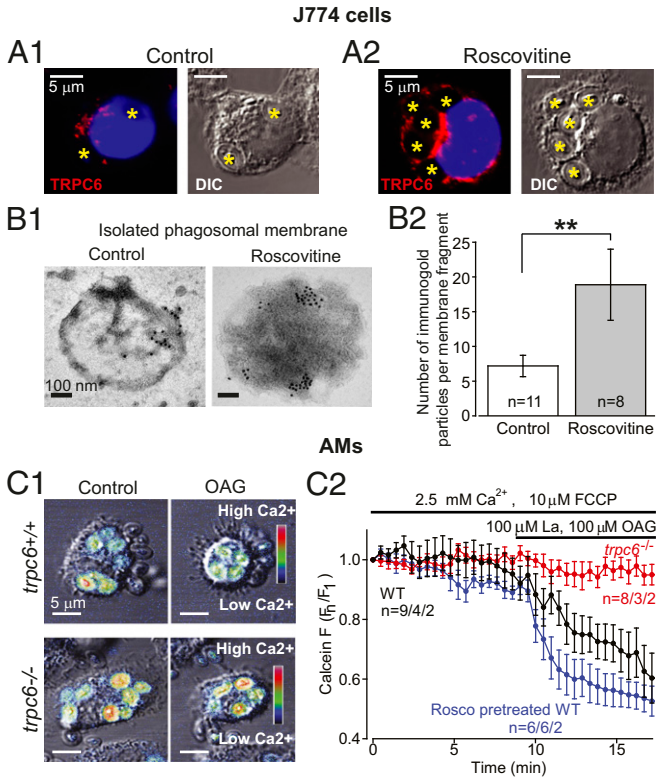

Fig. 6. Functional TRPC6 expression in AMs and J774 cells. (*A1*) Confocal immunofluorescence images of TRPC6 distribution in representative J774 cells following zymosan particle phagocytosis (engulfed zymosan particles are marked with an asterisk). (*A2*) Following (R)-roscovitine (20 μM) exposure, TRPC6 colocalizes and surrounds the zymosan particles in a ring-like manner. (*B1*) Immunogold labeling of TRPC6 on isolated phagosomal membranes from nontreated as well as (R)-roscovitine–treated J774 cells. (Scale bar, 100 nm.) TRPC6 antibody staining was undetectable in *trpc6*$^{-/-}$ AMs, demonstrating antibody specificity for TRPC6 (see Fig. S3). (*B2*) Comparative summary of immunogold labeling of isolated phagosomal membrane fragments with equivalent area. Data were analyzed for $n = 11$ phagosomal fragments (images) under control conditions and $n = 8$ fragments for cells pretreated with (R)-roscovitine before particle uptake. Significance level: $^{**}P < 0.01$ (Fisher's exact test). (*C1* and *C2*) Calcein-monitored Ca^{2+} changes in phagosomes before and after (R)-roscovitine or OAG in *trpc6*$^{+/+}$ and *trpc6*$^{-/-}$ AMs: (*C1*) Merged confocal fluorescent and DIC images of phagocytosed zymosan particles in *trpc6*$^{+/+}$ (*Upper*) and *trpc6*$^{-/-}$ (*Lower*) AMs. Zymosan particles were preloaded with calcein (100 μM) and added to cells in bath solution containing 2.5 mM Ca^{2+} and the protonophore FCCP (10 μM). Upon stimulation with OAG (100 μM), there was a rapid loss of Ca^{2+} from the phagosomes of *trpc6*$^{+/+}$cells, but not from *trpc6*$^{-/-}$ cells. Calcein fluorescence images were depicted with a heat scale lookup table and merged with DIC images and displayed as before (Control) and after exposure to OAG. (*C2*) Time course of calcein fluorescence intensity change in phagosomes from: *trpc6*$^{-/-}$, *trpc6*$^{+/+}$, and *trpc6*$^{+/+}$ cells pretreated with (R)-roscovitine (20μM) (with indicated numbers of analyzed phagosomes per cells per mice). Lanthanum (100 μM) was coapplied with OAG to block plasmalemmal TRPC6 channel activation and preserve intracellular Ca^{2+} levels; 10 μM FCCP was added to prevent phagosomal acidification in the presence of the pH-sensitive calcein. Sample size: n = phagosomes per cells per mice.

from wild-type cells (Fig. 6*C*). As shown in Fig. 6 *C*, *2*, wild-type cells treated with 20 μM (R)-roscovitine showed an enhanced kinetic loss of fluorescence over wild-type. Phagosomes in *trpc6*$^{-/-}$ cells showed no loss in Ca^{2+}-dependent calcein fluorescence over the same time period demonstrating directly the functional role of TRPC6 activation in phagosomal membranes.

The activation of an OAG-sensitive current, TRPC6, at both the plasma and phagosomal membranes in the presence of OAG and (R)-roscovitine would predict that (R)-roscovitine might be acting indirectly through a GPCR of unknown identity. Such receptors are plentiful on the macrophage surface and include formyl peptide, adenosine, and purinergic, as well as chemokine receptors (33–36). If (R)-roscovitine acts through a GPCR, our prediction would be that we should see measureable DAG generation. The expression of a DAG-sensitive CFP/YFP FRET reporter (DAGR) (37) in J774 cells, allowed us to measure the kinetics of DAG generation in the response to 50 μM (R)-roscovitine (working concentration for J774 cells) and 100 μM OAG (Fig. 7 *A* and *B*). In these experiments, OAG acts as a positive control for DAGR expression and function, as both DAG and its analog OAG bind to the DAGR. OAG allowed us to estimate the maximum DAGR response. Both OAG and (R)-roscovitine induced FRET signals, indicative of a (R)-roscovitine–induced GPCR-mediated response. To further confirm that DAG was generated through a GPCR pathway, we repeated the experiment in the presence of pertussis toxin (PTX) (Fig. 7*C*). The ability of PTX to inhibit (R)-roscovitine-induced DAG generation in the J774 cells confirmed the interaction of (R)-roscovitine with an unidentified GPCR and associated signaling cascade.

(R)-Roscovitine Induces an Increase in the Frequency of Intracellular Ca^{2+} Oscillations, Which Is Dependent Upon External Ca^{2+}. If (R)-roscovitine opens a Ca^{2+}-permeable TRPC6 channel, it follows that we should observe this interaction as an increase in internal Ca^{2+} dependent upon (R)-roscovitine exposure. In Fluo-4AM imaging experiments carried out on both murine and human AMs, exposure to (R)-roscovitine led to increases in the frequency of spontaneous Ca^{2+} oscillations (Fig. 8 *A* and *B*). Ca^{2+} oscillations have been previously described in macrophages, however only in association with phagocytosis (38, 39). As in the electrophysiological studies, the TRPC6 agonist, OAG, mimicked (R)-roscovitine in increasing Ca^{2+} spike frequency (Fig. 8*C*). Oscillations decayed rapidly following the removal of Ca^{2+} from the extracellular solution, indicating their dependence upon extracellular Ca^{2+} influx. Application of (R)-roscovitine did not rescue the decline in oscillations after extracellular Ca^{2+} withdrawal (Fig. S5), consistent with our electrophysiological observations demonstrat-

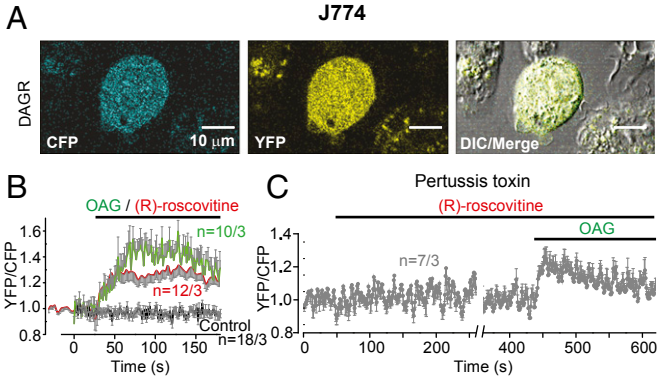

Fig. 7. (R)-roscovitine generates DAG via a PTX-sensitive GPCR activation pathway. (*A*) Representative cellular expression of the FRET-based CFP/YFP DAG-reporter in J774 cell fluorescent and DIC images. (Scale bar, 10 μm.) (*B*) Time course of (R)-roscovitine–generated DAG production in transfected J774 cells following exposure to 50 μM (R)-roscovitine (red trace, 12 cells) or 100 μM OAG (green trace, 10 cells) treatment. The gray trace represents cellular responses in DAG reporter-expressing cells in the absence of drug treatment (18 cells). (*C*) (R)-roscovitine (50 μM) failed to elicit DAG production in J774 cells treated with PTX (300 ng/mL) overnight. Subsequent addition of OAG (100 μM) elicited maximum DAG reporter detection and provided a control for DAGR expression (seven cells). Mean FRET ratio values are indicated as solid lines and error bars in gray indicate SEM. Number of the cells and experiments is given in Table S4 and indicated in the plots as n = cells per experiments.

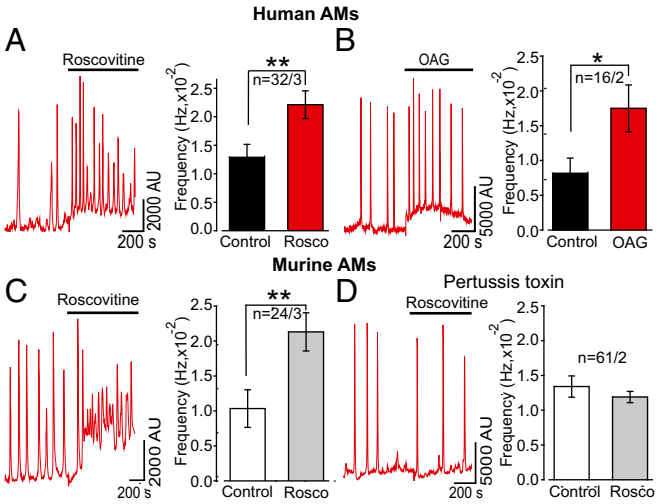

Fig. 8. Intracellular Ca^{2+} oscillations induced by (R)-roscovitine are dependent upon GPCR activation and mimicked by the DAG analog, OAG, in human and murine AMs. Experiments were carried out on cultured AMs using Fluo-4AM as the Ca^{2+} indicator dye within 2 d after isolation. (*A*) Representative traces showing increases in spontaneous Ca^{2+} oscillation frequency in human AMs (n = 32 cells, 3 BAL human samples) following exposure to (R)-roscovitine (50 μM, 15 min). In any given field, only a subpopulation of cells exhibited oscillatory behavior. In human AMs, 35% exhibited spontaneous oscillations, whereas 18% of murine AMs showed the same behavior. The (R)-roscovitine effect was most visible on oscillating cells; therefore, we confined our analysis to cells with spontaneous oscillations. There was no obvious morphological difference between oscillating and nonoscillating cells at rest. (*B*) Data from murine AMs (n = 24 cells, 3 mice) are as described for human cells in *A*. (*C*) Representative Ca^{2+} oscillations and frequency analysis of human AMs in response to application of 50 μM OAG (n = 16 cells, 2 BAL human samples). (*D*) Representative Ca^{2+} oscillations and frequency analysis of murine macrophages pretreated for 6 h with 300 nM PTX prior application of 50 μM (R)-roscovitine (n = 61 cells, 2 mice). Significance levels: $*P < 0.05$, $**P < 0.01$ (two-way ANOVA). Number of mice and BAL in each experiment is given in Table S4 and indicated in the plots as n = cells per mice or cells per BAL.

ing (R)-roscovitine's indirect activation of TRPC6 Ca^{2+}-permeable channels through a GPCR signaling pathway. Application of OAG in the absence of extracellular Ca^{2+} also failed to enhance Ca_i oscillation frequency (Fig. S5), a finding consistent with their genesis through TRPC6 activation and subsequent Ca^{2+} influx.

To further elucidate whether (R)-roscovitine gates a Ca^{2+}-selective pathway directly from the external surface or indirectly (i.e., at the cytoplasmic side through a GPCR generating IP_3 and DAG to activate TRPC6), we determined whether the (R)-roscovitine–enhanced Ca^{2+} oscillations were dependent upon G-protein activation. If (R)-roscovitine gates the TRPC6 channel directly independent of a second messenger-signaling pathway, inhibiting G-protein activation with PTX should have no effect on the frequency or amplitude of Ca^{2+} oscillations. To test this, cells were pretreated with PTX (300 ng/mL) for at least 6 h and examined for (R)-roscovitine enhancement of oscillatory responses. Data from these experiments, summarized in Fig. 8*D*, demonstrated that PTX treatment prevented the (R)-roscovitine–enhanced increase in Ca^{2+} oscillation frequency, consistent with (R)-roscovitine acting through a GPCR. (R)-roscovitine–induced oscillations were dependent upon the expression of TRPC6 failing to enhance Ca^{2+} oscillation frequency in *trpc6*$^{-/-}$ cells (Fig. 9).

Direct Measurement of (R)-Roscovitine Induced Exocytotic Insertion of TRPC6 into the Plasma Membrane Following GPCR Activation in Human AMs. Quantification of the increase in TRPC6 plasma membrane localization following (R)-roscovitine treatment was determined in human AMs using an antibody directed at the extracellular domain of the protein, α-rTRPC6$_{573–586}$. Fig. 10*A* shows immunocytochemical surface labeling of representative cells under control conditions and following treatment with (R)-roscovitine and OAG, both shown to enhance current activation and Ca^{+} signaling. The formyl peptide fMLF and 4-bromo-A23187, both agents known to mobilize Ca^{2+}, also showed significant enhancement of surface localization (Fig. S6). Quantification of the enhancement of surface labeling showed significant increases in surface staining for all compounds over that seen at steady-state in control cells (Fig. 10*B*), indicating that any stimulus capable of generating increases in DAG and Ca^{2+} might also be efficient in promoting both phagosomal acidification and killing, as was seen for fMLF in the initial acidification screen (Fig. 1 *B* and *C*).

The membrane dye FM1-43 has been used extensively to track exocytosis, endocytosis, and recycling of secretory granules or vesicles (40). FM1-43 molecules, when present in the extracellular solution, insert into the plasma membrane and are internalized during endocytosis. The newly formed vesicles retain dye in their inner leaflet as well as in the vesicle lumen while in the cytoplasmic compartment (Fig. 10*C*). When stimulated to undergo exocytosis in a dye-free medium, the vesicles lose their fluorescent content (Fig. 10*C*). Thus, the exocytotic response is measured as a decrease in intracellular fluorescence or destaining. We used this technique to measure the kinetics of the exocytotic translocation of vesicles upon treatment with either (R)-roscovitine or OAG (Fig. 10*D*). In the presence of extracellular Ca^{2+}, both (R)-roscovitine and OAG induced significant destaining of the AM intracellular compartment over that observed in the absence of drug. The exocytotic vesicle insertion was dependent upon external Ca^{2+}, as seen in Fig. 10*E*. Thus, although this technique does not allow for the identification of the vesicle-type or cargo, the correlation between immunocytochemical data (Fig. 10*A*), electrophysiological current activation, and Ca^{2+} signaling support the hypothesis that vesicle fusion is responsible for the enhancement TRPC6 plasma membrane expression as schematically represented in Fig. 10*F*. G protein-mediated activation of phospholipase C leads to the production of DAG and IP_3. DAG opens Ca^{2+}-permeable, plasmalemmal TRPC6 channels, whereas IP_3 binds to its cognate receptor (IP_3R) on the endoplasmic reticulum, triggering release of Ca^{2+} from internal stores. The consequent rapid rise in cytoplasmic Ca^{2+} facilitates the translocation and fusion of TRPC6-containing vesicles to the plasma membrane.

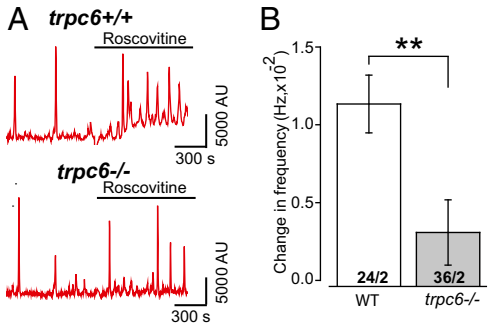

Fig. 9. (R)-roscovitine–induced increase in internal Ca^{+2} oscillations is dependent upon TRPC6 expression. (*A*) Representative Ca^{2+} oscillations from *trpc6*$^{+/+}$ and *trpc6*$^{-/-}$ mice before and following exposure to 50 μM (R)-roscovitine. (*B*) Summary of the (R)-roscovitine–induced increase in Ca^{2+} oscillation frequency comparing first and last 200-s bin time periods [before and after application of (R)-roscovitine] observed in *trpc6*$^{+/+}$ (n = 24 cells, 2 mice) and trpc6$^{-/-}$ cells (n = 36 cells, 2 mice). Significance level: $**P < 0.01$ (two-way ANOVA).

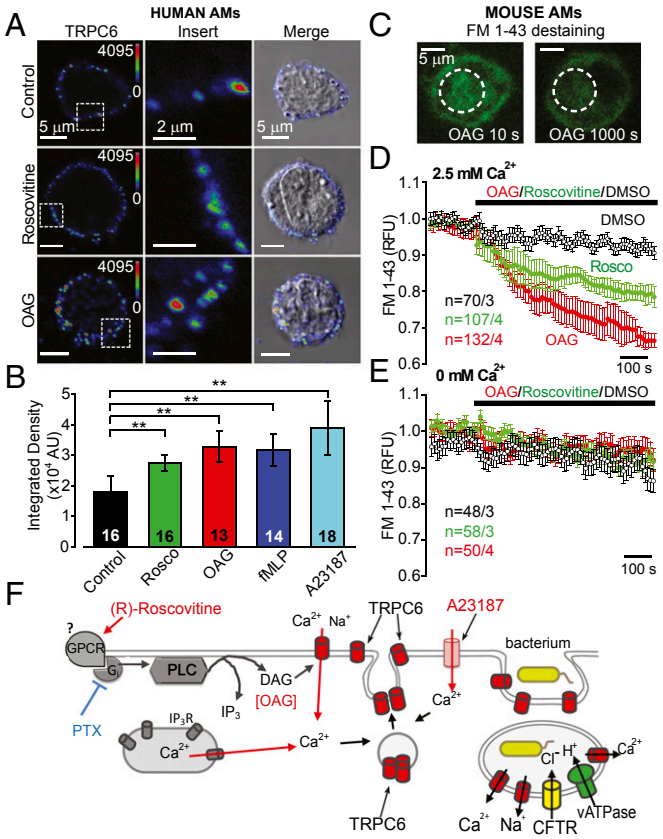

Fig. 10. (R)-roscovitine as well as OAG induce exocytotic insertion of TRPC6 channels into the plasma membrane. (*A*) Human AMs were stained with α-rTRPC6$_{573–586}$; cells were treated with either 20 μM (R)-roscovitine or 100 μM OAG for 15 min at 37 °C before fixation for microscopy. A color gradient scheme (Rainbow) was used to highlight increased density of TRPC6 surface labeling following (R)-roscovitine or OAG treatment. A 5 × 5-μm square of surface staining was highlighted in the *Left* column of images and expanded in the *Center* column to clearly illustrate denser TRPC6 surface labeling. The *Right* column depicts an overlay of the TRPC6 immunofluorescence image with its corresponding DIC image. (*B*) Comparative summary of surface TRPC6 expression quantified as mean fluorescence integrated density (area × mean value of fluorescence intensity) ± SEM. Significance level: $^{**}P \leq 0.01$ (Mann–Whitney rank sum test); cell number in center of the bars. (*C*) Representative images of murine AMs, loaded with the membrane marker FM1-43, before (10 s) and after (1,000 s) application of OAG. Note the significant decrease in cytoplasmic staining following OAG treatment which reflects the exocytotic release of FM1-43 into the bath following exocytosis. (*D*) Comparative time-dependent changes in cytoplasmic FM1-43 fluorescence following exposure of murine AMs to 100 μM OAG or 50 μM (R)-roscovitine in 2.5 mM Ca^{2+}-containing bath solution. (*E*) In Ca^{2+}-free bath solution no significant temporal changes in FM1-43 fluorescence were observed during OAG or (R)-roscovitine treatments. (*F*) Proposed model for (R)-roscovitine interaction with an as yet unidentified GPCR and the downstream signaling pathway leading to the exocytotic insertion of vesicular TRPC6 channels into plasma membrane and their subsequent activation by DAG. Sample size (*n* = cells per mice) indicated for each condition and detailed in Table S4.

These same channels are incorporated into phagosomal membranes upon bacterial engulfment.

Causal Relationship Between TRPC6 and Phagosome Acidification. Although it is clear that (R)-roscovitine is causally related to TRPC6 activation and translocation, the next set of experiments were directed at determining whether TRPC6 expression is causally related to enhancement of phagosomal function. If both CFTR and TRPC6 subserve the same charge-shunt function in the phagosome, eliminating the expression of one of the channels would still leave the other to facilitate acidification. Before proceeding, we carried out experiments to determine if CFTR is expressed in *trpc6*$^{-/-}$ cells and vice versa, the results of which are given in Fig. S7. TRPC6 current was activated by OAG in *cftr*$^{-/-}$ cells and expression confirmed by immuno-localization, as seen in Fig. S7*A*. Conversely, the cAMP-elevating mixture elicited current in the *trpc6*$^{-/-}$ cells, corroborating positive immunostaining for CFTR in Fig. S7*B*.

Given these findings, we used the CFTR inhibitor, CFTR$_{inh}$172, to reveal the effect of TRPC6 on acidification in the presence and absence of (R)-roscovitine. In Fig. 11*A* we compared the kinetics and magnitude of phagosomal acidification in wild-type AMs expressing both CFTR and TRPC6 (*cftr*$^{+/+}$/ *trpc6*$^{+/+}$). In these cells, phagosomes containing pHrodo-labeled zymosan particles failed to acidify in the presence of CFTR$_{inh}$172 (30 μM). Treatment of the cells with both CFTR$_{inh}$172 and (R)-roscovitine showed phagosomal acidification equal to or modestly enhanced over that observed in untreated control cells, allowing us to conclude that (R)-roscovitine–induced recovery of phagosomal function was not dependent upon CFTR activation. Similar experiments performed in *trpc6*$^{-/-}$ (*cftr*$^{+/+}$/*trpc6*$^{-/-}$) cells (Fig. 11*B*) revealed the unanticipated finding that the absence TRPC6 expression led to a significant decrease in phagosomal acidification over that observed in wild-type (*cftr*$^{+/+}$/ *trpc*$^{+/+}$) cells, indicating that both anion and cation channels participated in steady-state phagosomal function. As expected, the *trpc6*$^{-/-}$ cells were highly sensitive to CFTR$_{inh}$172. Finally, (R)-roscovitine in the presence of CFTR$_{inh}$172 failed to rescue acidification in the *trpc6*$^{-/-}$ cells, showing a direct and causal relationship between (R)-roscovitine, TRPC6 expression, and phagosomal acidification.

Discussion

Resolution of chronic pulmonary infection in CF, as well as COPD, asthma, and tuberculosis, without the use of antimicrobials is a necessity in a clinical environment faced with increasing bacterial antibiotic resistance. Our data demonstrate that (R)-roscovitine

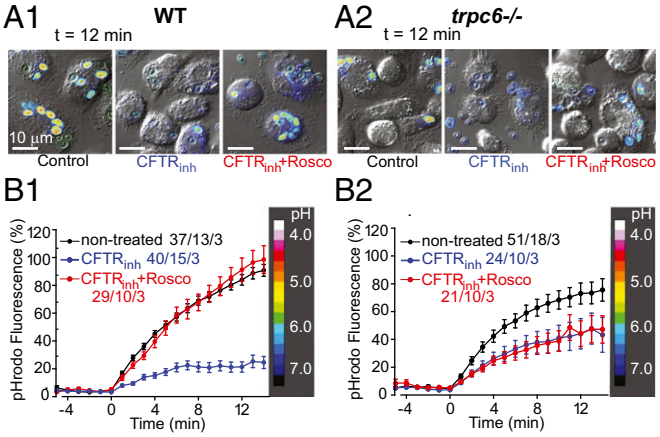

Fig. 11. (R)-Roscovitine enhances acidification in CFTR$_{inh}$172-treated *trpc6*$^{+/+}$ (wild-type) cells but not in the *trpc6*$^{-/-}$ cells. (*A1* and *A2*) Representative fluorescence-DIC image overlays of *trpc6*$^{+/+}$ (wild-type) (*A1*) and *trpc6*$^{-/-}$ (*A2*) AMs with pHrodo red-labeled zymosan at *t* = 12 min following loading under three conditions: DMSO control, 10 μM CFTR$_{inh}$172, and 10 μM CFTR$_{inh}$172 plus 20 μM (R)-roscovitine. (*B1*) Time course of phagosomal acidification in wild-type AMs under the following conditions: DMSO control (black trace), 10 μM CFTR$_{inh}$172 (blue trace), 10 μM CFTR$_{inh}$172 plus 20 μM (R)-roscovitine (red trace). (*B2*) Time course of phagosomal acidification in *trpc6*$^{-/-}$ AMs under the same conditions as in *B1*. Heat scale along the right *y* axis correlates changes in pHrodo red zymosan color intensities in the above images with a calibrated pH value range. Data are displayed as means ± SEM. Sample size (*n* = phagosomes/cells/mice) indicated for each condition and detailed in Table S4.

and related metabolites and derivatives rescue phagocytic function in CF pulmonary macrophages, which is independent of kinase inhibition and of CFTR expression. Our data, which are modeled in Fig. S8, are consistent with a mechanism whereby (R)-roscovitine binds to an as yet unidentified GPCR-activating downstream signaling molecules, including phospholipase C, generating DAG and IP_3, giving rise to Ca^{2+} mobilization from external as well as internal sites. Sequelae include incorporation into and activation of Ca^{2+}-permeable TRPC6 channels in the plasma, as well as phagosomal membrane and mobilization and fusion of endolysosomal vesicles to the maturing phagosome contributing V-ATPase (Fig. S9), all events leading to luminal phagosomal charge neutralization and enhanced acidification, the prelude to enhanced bacterial killing. Inhibition of (R)-roscovitine action by PTX strongly suggests that it is acting through a GPCR-mediated pathway. Ligation of selected subsets of GPCRs is linked to the assembly and activation of NADPH oxidase and the release of free radicals associated with bacterial killing in the phagosomes of blood neutrophils (41), and to a much lesser extent in tissue macrophages (42). Stimulus-induced production of oxidants in tissue macrophages has been shown to be ∼110-fold less than that observed for blood phagosomes of blood neutrophils (43). In agreement with these findings, we were unable to observe an increase in oxidant (ROS) production in murine AMs challenged with bacteria following exposure to (R)-roscovitine (Fig. S10*B*), nor we were able to see a difference in stimulus-induced generation of ROS production between the murine AM genotypes, $cftr^{+/+}$ and $cftr^{-/-}$, either in the presence or absence of (R)-roscovitine (Fig. S10). We have previously shown that murine $cftr^{-/-}$ AMs are not defective in ROS production but are defective in microbicidal function (3), strongly suggesting that other microbicidal enzymatic effectors contributed by lysosomal fusion and activated in the acidic environment of the phagosome play a significant role in bacterial killing. Although both human and murine CF lung macrophages seem to be intrinsically defective in bacterial killing, there is disagreement in the literature as to whether CFTR dysfunction impairs the contribution of ROS production to *P. aeruginosa* killing (44, 45) and may well be a function of species and tissue source.

Although we were unable to demonstrate that (R)-roscovitine acted as a corrector for the trafficking defect in the mutant protein, as has been previously reported (46), our electrophysiological experiments on isolated cells did demonstrate that (R)-roscovitine activated a TRPC6 conductance, a response which was absent in $trpc6^{-/-}$ cells. TRPC6 channels are translocated to the plasma membrane upon (R)-roscovitine stimulation and appear to remain in the membrane so long as the stimulus is present. The concept of TRPC6 mobilization to the plasma membrane as a function of G-protein receptor activation has been documented for the muscarinic receptor in heterologous expression systems (47, 48), as well as for lysophosphatidylcholine's inhibition of mouse aortic endothelial cell migration (49), and serves as a template for expression regulation in the AM. When incorporated into the phagosomal membrane, TRPC6 would serve as charge-shunt pathway, leading to the loss of luminal cations and supporting enhanced V-ATPase proton translocation in the development of the antimicrobial environment of the phagosomal compartment. Our data demonstrate that (R)-roscovitine generated DAG could activate plasma membrane resident TRPC6 channels, providing for a local Ca^{2+} influx creating a (R)-roscovitine–driven positive feedback loop, supporting enhanced translocation of endosomal Ca^{2+} permeable TRPC6 channels to the plasma membrane or alternatively to the phagosomal membrane directly, as well as possibly driving lysosomal fusion to phagosomes. Increasing expression of TRPC6 at the plasma membrane would contribute to a microdomain of increased Ca^{2+} around the phagocytic cup and lead to enhanced incorporation of the Ca^{2+} conductance into the maturing phagosome. Plasmalemmal TRPC6 incorporated into the phagosomal membrane during particle uptake is then well positioned to act as a charge-shunt pathway, supporting cation movement out of the phagosome, amplifying V-ATPase–driven acidification during the maturation process. In an unanticipated finding, we have shown that TRPC6 appears to participate in phagosomal acidification in the nondrug-treated AM, as well as rescue AM phagosomal function in drug-treated cells defective in CFTR function.

TRPC6 channels are present at low density in the plasma membrane of wild-type and CFTR-deficient cells, as seen in Fig. 10 and Fig. S7*A*. Their activation contributes to a significant fraction of phagosomal acidification in wild-type cells (Fig. 11*B*), which may be because of a regulatory interaction between CFTR and TRPC6, as seen the in the studies of Tabeling et al. (32) for pulmonary artery smooth-muscle cells. TRPC6 requires GPCR activation to generate not only DAG as an agonist for the channel, but also Ca^{2+} to induce channel translocation and insertion. If there is a protein–protein interaction between TRPC6 and CFTR, as in the Tabeling et al. studies, which enhances TRPC6 opening in the wild-type cells, GPCR activation may be essential for channel opening in the CFTR-deficient cells.

Our data examining the optimization of phagosomal function by (R)-roscovitine takes advantage of animal models available for the study of pulmonary inflammation in CF. It serves, however, in a broader sense as a template for the exploration of novel mechanisms, which might resolve inflammation in a host-directed manner in a diversity of pulmonary diseases, including tuberculosis, COPD, and asthma. Knowledge of the signaling and fusion events potentially available to reprogram the phagosome for enhanced microbicidal function is critical for the success of this strategy. The plethora of GPCRs in resident pulmonary macrophages (36) that may be linked to ion channel function provides a rich source for potential therapeutic approaches to macrophage-mediated disease. This theory is further supported by recent report that TRPML1 channels are similarly involved in charge shunting for large phagosomes in bone marrow macrophages (5), and suggests multiple alternatives to CFTR may exist for mitigating bactericidal defects in CF, as well as multiple acidification mechanisms in diverse macrophage lineages.

Materials and Methods

See *SI Materials and Methods* for details of experimental procedures and summarized data on sample size (number of particles per cells) and number of experiments (human or mice) in Table S4.

Animals. All studies detailed herein conform entirely to the principles and regulations set forth by the Animal Welfare Act, the National Institutes of Health *Guide for the Care and Use of Laboratory Animals* (50), and were approved by the University of Chicago Institutional Animal Care and Use Committee.

BAL from Humans. All procedures were performed on consenting adults following a protocol approved by The University of Chicago Institutional Review Board.

ACKNOWLEDGMENTS. The authors thank Dr. Rong Ma (University of North Texas, Fort Worth), who generously offered the use of his laboratory and animals in the first experiments involving the $trpc6^{-/-}$ mice; Drs. Radmila Sarac, Theodore Karrison, and Olga Zaborina, for many helpful conversations over the course of the study; Dr. G. Thinakaran for the gift of the many vesicle-directed antibodies; Yimei Chen in the Electron Microcopy Core at the University of Chicago, for his expertise; Dr. Richard D. Ye (University of Illinois at Chicago) for his help in the initial experiments examining whether (R)-roscovitine acted through the formyl peptide receptors; and Dr. Partha Kasturi (University of Kansas) for providing the initial experiments and analysis examining whether (R)-roscovitine modulated V-ATPase activity. This work was supported by National Institutes of Health Grants R01 GM36823, R01 HL125076, and R01 DK080364 (to D.J.N.); Cystic Fibrosis Foundation 12 and 13PO (to D.J.N.); and by the "Intramural Research Program of the NIH", Project Z01-ES-101684 (to L.B.).

1. Lieberman TD, et al. (2014) Genetic variation of a bacterial pathogen within individuals with cystic fibrosis provides a record of selective pressures. *Nat Genet* 46(1):82–87.
2. Dettman JR, Rodrigue N, Aaron SD, Kassen R (2013) Evolutionary genomics of epidemic and nonepidemic strains of *Pseudomonas aeruginosa*. *Proc Natl Acad Sci USA* 110(52):21065–21070.
3. Di A, et al. (2006) CFTR regulates phagosome acidification in macrophages and alters bactericidal activity. *Nat Cell Biol* 8(9):933–944.
4. Deriy LV, et al. (2009) Disease-causing mutations in the cystic fibrosis transmembrane conductance regulator determine the functional responses of alveolar macrophages. *J Biol Chem* 284(51):35926–35938.
5. Samie M, et al. (2013) A TRP channel in the lysosome regulates large particle phagocytosis via focal exocytosis. *Dev Cell* 26(5):511–524.
6. Goh GY, et al. (2011) Presynaptic regulation of quantal size: K^+/H^+ exchange stimulates vesicular glutamate transport. *Nat Neurosci* 14(10):1285–1292.
7. Steinberg BE, et al. (2010) A cation counterflux supports lysosomal acidification. *J Cell Biol* 189(7):1171–1186.
8. Damann N, Owsianik G, Li S, Poll C, Nilius B (2009) The calcium-conducting ion channel transient receptor potential canonical 6 is involved in macrophage inflammatory protein-2-induced migration of mouse neutrophils. *Acta Physiol (Oxf)* 195(1):3–11.
9. Nagasawa M, Nakagawa Y, Tanaka S, Kojima I (2007) Chemotactic peptide fMetLeuPhe induces translocation of the TRPV2 channel in macrophages. *J Cell Physiol* 210(3):692–702.
10. Link TM, et al. (2010) TRPV2 has a pivotal role in macrophage particle binding and phagocytosis. *Nat Immunol* 11(3):232–239.
11. Di A, et al. (2012) The redox-sensitive cation channel TRPM2 modulates phagocyte ROS production and inflammation. *Nat Immunol* 13(1):29–34.
12. Li S, Westwick J, Poll C (2003) Transient receptor potential (TRP) channels as potential drug targets in respiratory disease. *Cell Calcium* 33(5-6):551–558.
13. Banner KH, Igney F, Poll C (2011) TRP channels: Emerging targets for respiratory disease. *Pharmacol Ther* 130(3):371–384.
14. Dietrich A, Gudermann T (2014) TRPC6: Physiological function and pathophysiological relevance. *Handbook Exp Pharmacol* 222:157–188.
15. Baker KE, et al. (2014) Novel drug targets for asthma and COPD: Lessons learned from in vitro and in vivo models. *Pulm Pharmacol Ther* 29(2):181–198.
16. Finney-Hayward TK, et al. (2010) Expression of transient receptor potential C6 channels in human lung macrophages. *Am J Respir Cell Mol Biol* 43(3):296–304.
17. Antigny F, et al. (2011) Transient receptor potential canonical channel 6 links Ca^{2+} mishandling to cystic fibrosis transmembrane conductance regulator channel dysfunction in cystic fibrosis. *Am J Respir Cell Mol Biol* 44(1):83–90.
18. Hackam DJ, et al. (1997) Regulation of phagosomal acidification. Differential targeting of Na^+/H^+ exchangers, Na^+/K^+-ATPases, and vacuolar-type H^+-atpases. *J Biol Chem* 272(47):29810–29820.
19. Botelho RJ, et al. (2000) Localized biphasic changes in phosphatidylinositol-4, 5-bisphosphate at sites of phagocytosis. *J Cell Biol* 151(7):1353–1368.
20. Schepetkin IA, et al. (2008) Identification of novel formyl peptide receptor-like 1 agonists that induce macrophage tumor necrosis factor alpha production. *Mol Pharmacol* 74(2):392–402.
21. Meijer L, Raymond E (2003) Roscovitine and other purines as kinase inhibitors. From starfish oocytes to clinical trials. *Accounts Chem Res* 36:417–425.
22. Ip WK, et al. (2010) Phagocytosis and phagosome acidification are required for pathogen processing and MyD88-dependent responses to *Staphylococcus aureus*. *J Immunol* 184(12):7071–7081.
23. Sun-Wada GH, Tabata H, Kawamura N, Aoyama M, Wada Y (2009) Direct recruitment of H^+-ATPase from lysosomes for phagosomal acidification. *J Cell Sci* 122(Pt 14): 2504–2513.
24. Estacion M, Sinkins WG, Jones SW, Applegate MA, Schilling WP (2006) Human TRPC6 expressed in HEK 293 cells forms non-selective cation channels with limited Ca^{2+} permeability. *J Physiol* 572(Pt 2):359–377.
25. Inoue R, et al. (2001) The transient receptor potential protein homologue TRP6 is the essential component of vascular alpha(1)-adrenoceptor-activated $Ca^{(2+)}$-permeable cation channel. *Circ Res* 88(3):325–332.
26. Li SW, Westwick J, Poll CT (2002) Receptor-operated Ca^{2+} influx channels in leukocytes: A therapeutic target? *Trends Pharmacol Sci* 23(2):63–70.
27. Lockwich TP, et al. (2000) Assembly of Trp1 in a signaling complex associated with caveolin-scaffolding lipid raft domains. *J Biol Chem* 275(16):11934–11942.
28. Treviño CL, Serrano CJ, Beltrán C, Felix R, Darszon A (2001) Identification of mouse trp homologs and lipid rafts from spermatogenic cells and sperm. *FEBS Lett* 509(1): 119–125.
29. Torihashi S, Fujimoto T, Trost C, Nakayama S (2002) Calcium oscillation linked to pacemaking of interstitial cells of Cajal: Requirement of calcium influx and localization of TRP4 in caveolae. *J Biol Chem* 277(21):19191–19197.
30. Sanxaridis PD, et al. (2007) Light-induced recruitment of INAD-signaling complexes to detergent-resistant lipid rafts in *Drosophila* photoreceptors. *Mol Cell Neurosci* 36(1): 36–46.
31. Bardell TK, Barker EL (2010) Activation of TRPC6 channels promotes endocannabinoid biosynthesis in neuronal CAD cells. *Neurochem Int* 57(1):76–83.
32. Tabeling C, et al. (2015) CFTR and sphingolipids mediate hypoxic pulmonary vasoconstriction. *Proc Natl Acad Sci USA* 112(13):E1614–E1623.
33. Lattin J, et al. (2007) G-protein-coupled receptor expression, function, and signaling in macrophages. *J Leukoc Biol* 82(1):16–32.
34. Lattin JE, et al. (2008) Expression analysis of G protein-coupled receptors in mouse macrophages. *Immunome Res* 4:5.
35. Varani K, et al. (2010) Oxidative/nitrosative stress selectively altered A(2B) adenosine receptors in chronic obstructive pulmonary disease. *FASEB J* 24(4):1192–1204.
36. Groot-Kormelink PJ, Fawcett L, Wright PD, Gosling M, Kent TC (2012) Quantitative GPCR and ion channel transcriptomics in primary alveolar macrophages and macrophage surrogates. *BMC Immunol* 13:57.
37. Violin JD, Zhang J, Tsien RY, Newton AC (2003) A genetically encoded fluorescent reporter reveals oscillatory phosphorylation by protein kinase C. *J Cell Biol* 161(5): 899–909.
38. Kruskal BA, Maxfield FR (1987) Cytosolic free calcium increases before and oscillates during frustrated phagocytosis in macrophages. *J Cell Biol* 105(6 Pt 1):2685–2693.
39. Myers JT, Swanson JA (2002) Calcium spikes in activated macrophages during Fcgamma receptor-mediated phagocytosis. *J Leukoc Biol* 72(4):677–684.
40. Brumback AC, Lieber JL, Angleson JK, Betz WJ (2004) Using FM1-43 to study neuropeptide granule dynamics and exocytosis. *Methods* 33(4):287–294.
41. Sun L, Ye RD (2012) Role of G protein-coupled receptors in inflammation. *Acta Pharmacol Sin* 33(3):342–350.
42. Nunes P, Demaurex N, Dinauer MC (2013) Regulation of the NADPH oxidase and associated ion fluxes during phagocytosis. *Traffic* 14(11):1118–1131.
43. Haugen TS, Skjønsberg OH, Kähler H, Lyberg T (1999) Production of oxidants in alveolar macrophages and blood leukocytes. *Eur Respir J* 14(5):1100–1105.
44. Cifani N, et al. (2013) Reactive-oxygen-species-mediated P. aeruginosa killing is functional in human cystic fibrosis macrophages. *PLoS One* 8(8):e71717.
45. Zhang Y, Li X, Grassmé H, Döring G, Gulbins E (2010) Alterations in ceramide concentration and pH determine the release of reactive oxygen species by Cftr-deficient macrophages on infection. *J Immunol* 184(9):5104–5111.
46. Norez C, et al. (2006) Rescue of functional delF508-CFTR channels in cystic fibrosis epithelial cells by the alpha-glucosidase inhibitor miglustat. *FEBS Lett* 580(8): 2081–2086.
47. Cayouette S, Lussier MP, Mathieu EL, Bousquet SM, Boulay G (2004) Exocytotic insertion of TRPC6 channel into the plasma membrane upon Gq protein-coupled receptor activation. *J Biol Chem* 279(8):7241–7246.
48. Cayouette S, et al. (2010) Involvement of Rab9 and Rab11 in the intracellular trafficking of TRPC6. *Biochim Biophys Acta* 1803(7):805–812.
49. Chaudhuri P, et al. (2008) Elucidation of a TRPC6-TRPC5 channel cascade that restricts endothelial cell movement. *Mol Biol Cell* 19(8):3203–3211.
50. Committee on Care and Use of Laboratory Animals (1996) *Guide for the Care and Use of Laboratory Animals* (Natl Inst Health, Bethesda), DHHS Publ No (NIH) 85–23.